2017 IEEE MTT-S International Conference on Numerical Electromagnetic and Multiphysics Modeling and Optimization for RF, Microwave, and Terahertz Applications (NEMO) (NEMO2017) , 17-19 May, 2017

Face Centered Anisotropic Surface Impedance Boundary Conditions in FDTD:

Improved performance of staircased mesh for shielding problems

J. F. Dawson, I. D. Flintoft, S. A. Bourke and M. P. Robinson
Department of Electronics
University of York
York, UK
john.dawson@york.ac.uk

M. R. Cabello and S. G. Garcia
Department of Electromagnetism and Matter Physics
University of Granada
Granada, Spain
salva@ugr.es

J. Alvarez
Airbus Defence and Space
28906 Getafe, Spain
jesus.g.alvarez@airbus.com

***Abstract*—We present a new face centered approach to the collocation of the fields for the application of a surface impedance boundary condition (SIBC). This approach deals with the ambiguities in the surface normal that arise at the edges on stair-cased surfaces.. The accuracy of the new scheme is compared to edge based and conformal approaches using both planar sheet and spherical shell test cases. Stair-casing effects are evaluated and the face-centered scheme exhibits significantly less error than the edge based approach.**

Keywords—computational electromagnetics, electromagnetic shielding, thin boundary

I. Introduction

Surface impedance boundary conditions (SIBCs) are widely used to represent thin shielding materials in transmission line-matrix (TLM) [1] and finite difference time-domain (FDTD) full-wave computational electromagnetics codes [2]. A wide range of methods have been applied in FDTD simulations and a review of recent developments can be found in [3]. Careful treatment of the intersection of SIBC faces is necessary in order to resolve the inherent ambiguity of the surface normal on stair-cased edges when curved surfaces are approximated on a structured mesh. Conformal algorithms have also been developed [4], [5], however, these techniques are more computationally expensive and a trade-off between efficiency and accuracy must be considered for any particular application.

In this paper we describe a new face-centered approach to implementing a two-sided SIBC in FDTD. This removes the ambiguity in the orientation of the surface normal on the SIBC edges and corners where the edge based approach has to be applied [6]. While much work has focused on planar sheet material validation cases for thin sheet boundaries we also show the behavior of the SIBC for more realistic curved surfaces. For the boundary time response we employ, cascaded second order digital filters, have previously been applied within the Transmission Line Matrix (TLM) method [1]. This offers more flexibility in optimizing the numerical performance of the discrete time algorithm than the recursive convolution algorithm, which is often used.

The research leading to these results has received funding from the UK Engineering and Physical Sciences Research Council (EPSRC) under the Flapless Air Vehicle Integrated Industrial Research (FLAVIIR) programme, grant GR/S71552/01, and from the European Community's Seventh Framework Programme, FP7/2007-2013, under grant agreement number. 205294 on the High Intensity Radio-frequency Field Synthetic Environment (HIRF SE) research project.

II. Implementation

An explicit update scheme is adopted for linking the SIBC algorithm into an FDTD code [7]. We impose the SIBC at the face centers of the primary mesh at the electric field sampling times using spatial interpolation. This makes the treatment of intersecting SIBC faces simple, at the expense of some extra averaging. Since the tangential electric fields lie in the plane of the SIBC boundary, the values to either side of the boundary must be stored separately on every face of the SIBC.

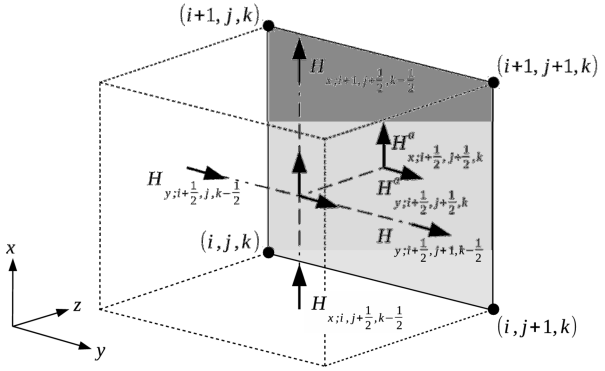

Fig. 1. Spatial interpolation of the tangential magnetic fields to the SIBC face centers for the electric field update on the z-low side of the z-normal face centered on (i+1/2,j+1/2,k). The SIBC face is shaded.

The SIBC for a z-normal face, centered on $(i+1/2\,,j+1/2\,,k)$ is given by:

$$\begin{bmatrix} E_x^a \\ E_x^b \\ E_y^a \\ E_y^b \end{bmatrix}^n_{i+\frac{1}{2},j+\frac{1}{2},k} = \bar{B}(\alpha)\mathrm{Z} \otimes \bar{A}(\alpha) \begin{bmatrix} H_x^a \\ H_x^b \\ H_y^a \\ H_y^b \end{bmatrix}^n_{i+\frac{1}{2},j+\frac{1}{2},k} \quad (1)$$

where a and b denote the two sides of the face, $\bar{A}(\alpha)$ and $\bar{B}(\alpha)$ are rotation matrices that are functions of the angle, α, between the principal axes of the material and x-axis of the mesh. Z is the impulse response matrix of the surface impedance boundary condition, and ⊗ denotes a convolution,

978-1-5090-4837-3/17/$31.00 ©2017 IEEE

achieved by means of the digital filter. The main difficulty is therefore the determination of the tangential magnetic fields at the correct sampling locations and times. The spatial interpolation scheme shown in Fig. 1 is first applied to allow the determination of the tangential components on the central normal axis of the face, half a cell either side of the boundary, at time $t = (n - 1/2)\Delta t$:

$$
\begin{aligned}
H^{n-\frac{1}{2}}_{x;i+\frac{1}{2},j+\frac{1}{2},k-\frac{1}{2}} &= \frac{1}{2}\left[H^{n-\frac{1}{2}}_{x;i,j+\frac{1}{2},k-\frac{1}{2}} + H^{n-\frac{1}{2}}_{x;i+1,j+\frac{1}{2},k-\frac{1}{2}}\right] \\
H^{n-\frac{1}{2}}_{x;i+\frac{1}{2},j+\frac{1}{2},k+\frac{1}{2}} &= \frac{1}{2}\left[H^{n-\frac{1}{2}}_{x;i,j+\frac{1}{2},k+\frac{1}{2}} + H^{n-\frac{1}{2}}_{x;i+1,j+\frac{1}{2},k+\frac{1}{2}}\right] \\
H^{n-\frac{1}{2}}_{y;i+\frac{1}{2},j+\frac{1}{2},k-\frac{1}{2}} &= \frac{1}{2}\left[H^{n-\frac{1}{2}}_{y;i+\frac{1}{2},j,k-\frac{1}{2}} + H^{n-\frac{1}{2}}_{y;i+\frac{1}{2},j+1,k-\frac{1}{2}}\right] \\
H^{n-\frac{1}{2}}_{y;i+\frac{1}{2},j+\frac{1}{2},k+\frac{1}{2}} &= \frac{1}{2}\left[H^{n-\frac{1}{2}}_{y;i+\frac{1}{2},j,k+\frac{1}{2}} + H^{n-\frac{1}{2}}_{y;i+\frac{1}{2},j+1,k+\frac{1}{2}}\right]
\end{aligned}
\tag{2}
$$

Then, to attain spatial and temporal co-location with the electric field at the face center, the magnetic fields on the boundary at $t = n\Delta t$ are estimated using :

$$
\begin{aligned}
H^{a;n}_{x;i+\frac{1}{2},j+\frac{1}{2},k} &\approx H^{n-\frac{1}{2}}_{x;i+\frac{1}{2},j+\frac{1}{2},k-\frac{1}{2}} \\
H^{b;n}_{x;i+\frac{1}{2},j+\frac{1}{2},k} &\approx H^{n-\frac{1}{2}}_{x;i+\frac{1}{2},j+\frac{1}{2},k+\frac{1}{2}} \\
H^{a;n}_{y;i+\frac{1}{2},j+\frac{1}{2},k} &\approx H^{n-\frac{1}{2}}_{y;i+\frac{1}{2},j+\frac{1}{2},k-\frac{1}{2}} \\
H^{b;n}_{y;i+\frac{1}{2},j+\frac{1}{2},k} &\approx H^{n-\frac{1}{2}}_{y;i+\frac{1}{2},j+\frac{1}{2},k+\frac{1}{2}}
\end{aligned}
\tag{3}
$$

This low order approximation limits the overall accuracy of the algorithm and has been suggested as a possible source of the long term instability sometimes observed in SIBC implementations in FDTD [8]. Nevertheless, since we are primarily interested in the behavior of a face-centered approach we apply the simple upwind approximation in (3) and take the boundary magnetic fields, which will be used after any rotation is applied, as input to the SIBC filters (1) to be

$$
\begin{bmatrix} H^a_x \\ H^b_x \\ H^a_y \\ H^b_y \end{bmatrix}^n_{i+\frac{1}{2},j+\frac{1}{2},k}
= \frac{1}{2}\begin{bmatrix}
H^{n-\frac{1}{2}}_{x;i,j+\frac{1}{2},k-\frac{1}{2}} + H^{n-\frac{1}{2}}_{x;i+1,j+\frac{1}{2},k-\frac{1}{2}} \\
H^{n-\frac{1}{2}}_{x;i,j+\frac{1}{2},k+\frac{1}{2}} + H^{n-\frac{1}{2}}_{x;i+1,j+\frac{1}{2},k+\frac{1}{2}} \\
H^{n-\frac{1}{2}}_{y;i+\frac{1}{2},j,k-\frac{1}{2}} + H^{n-\frac{1}{2}}_{y;i+\frac{1}{2},j+1,k-\frac{1}{2}} \\
H^{n-\frac{1}{2}}_{y;i+\frac{1}{2},j,k+\frac{1}{2}} + H^{n-\frac{1}{2}}_{y;i+\frac{1}{2},j+1,k+\frac{1}{2}}
\end{bmatrix}.
\tag{4}
$$

The tangential magnetic field-components adjacent to the SIBC are updated by the usual FDTD equations, but using the values for the tangential electric fields on the SIBC surface, for example,

$$
\begin{aligned}
H^{n+\frac{1}{2}}_{x;i,j+\frac{1}{2},k+\frac{1}{2}} &= H^{n-\frac{1}{2}}_{x;i,j+\frac{1}{2},k+\frac{1}{2}} \\
&+ C^{hxe}_{i,j+\frac{1}{2},k+\frac{1}{2}} \times \left[\begin{aligned}
&\frac{1}{\Delta z_k}\left\{E^n_{y;i,j+\frac{1}{2},k+1} - E^{b;n}_{y;i,j+\frac{1}{2},k}\right\} \\
&+\frac{1}{\Delta y_j}\left\{E^n_{z;i,j,k+\frac{1}{2}} - E^n_{z;i,j+1,k+\frac{1}{2}}\right\}
\end{aligned}\right]
\end{aligned}
\tag{5}
$$

where $C^{hxe}_{i,j+\frac{1}{2},k+\frac{1}{2}}$ is the standard magnetic field update coefficient [9]. Here the electric fields on the SIBC face edges are estimated from the average of those at the neighboring face centers, which are in turn determined by the by SIBC filter output (1) by using a simple two-point average:

$$
\begin{aligned}
E^{a;n}_{y;i,j+\frac{1}{2},k} &= \frac{1}{2}\left[E^{a;n}_{y;i-\frac{1}{2},j+\frac{1}{2},k} + E^{a;n}_{y;i+\frac{1}{2},j+\frac{1}{2},k}\right] \\
E^{b;n}_{y;i,j+\frac{1}{2},k} &= \frac{1}{2}\left[E^{b;n}_{y;i-\frac{1}{2},j+\frac{1}{2},k} + E^{b;n}_{y;i+\frac{1}{2},j+\frac{1}{2},k}\right]
\end{aligned}
\tag{6}
$$

III. Results

An analytic model for the impedance matrix of woven stainless steel wire mesh, which has an anisotropic impedance matrix, was used to test the anisotropic features of the SIBC algorithm [10]. The difference in shielding effectiveness (SE) between the TE and TM polarizations is about 25 dB. The agreement between analytic model, the partial fraction expansion fit used to generate the filter (sixth order in this case) and the FDTD simulation shown in Fig. 2 is excellent. The principal axes of the material can easily be orientated in any direction on a cell-by-cell basis using the implemented algorithm.

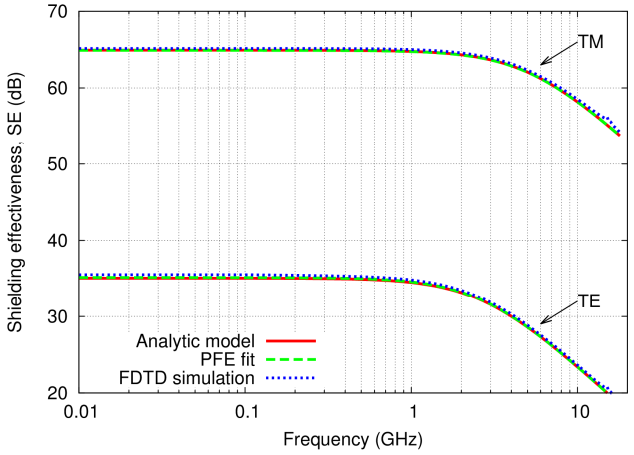

Fig. 2. Shielding effectiveness of an anisotropic wire mesh.

Fig. 3 shows a more complicated test case consisting of a 1 m radius hollow spherical shell made from a simple

conductive material. As the entire structure is curved, this case relies heavily on stair-case approximations, making it ideal for measuring the limits of SIBCs on structured meshes. A uniform plane-wave was used to illuminate the sphere and the SE at the center of the shell was determined. The mesh-size used in these FDTD models was 2 cm and the shell material is a 1 mm thick conductive sheet with a conductivity of 1 kS/m.

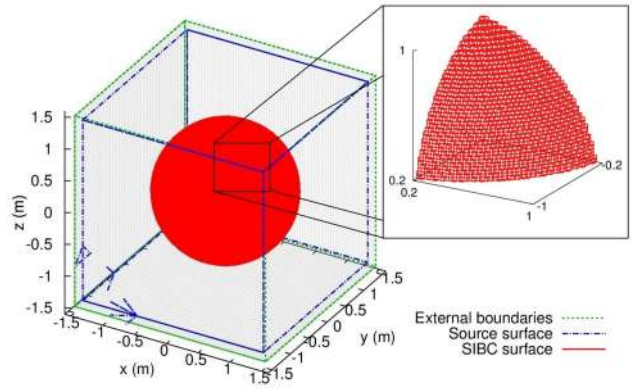

Fig. 3. Geometry of the hollow spherical shell test-case. The shell radius is 1 m and it is illuminated by a y-polarized plane-wave propagating along the x-direction generated by a total-field scattered-field boundary.

The new face centered approach is compared to the usual edge based approach implemented in [11] and also to results found with a conformal SIBC approach, based on the combination of the SIBC technique of [[12]] and the conformal method of [13] in Fig. 4. The results for the edge centered case shows an error of about 6 dB around the first resonance, whereas the face centered approach shows an error of approximately 3 dB. This is an appreciable increase in accuracy, but there is still a noticeable difference in comparison to the analytic model which is fully attributed to stair-casing errors as demonstrated by the superior accuracy of the conformal results.

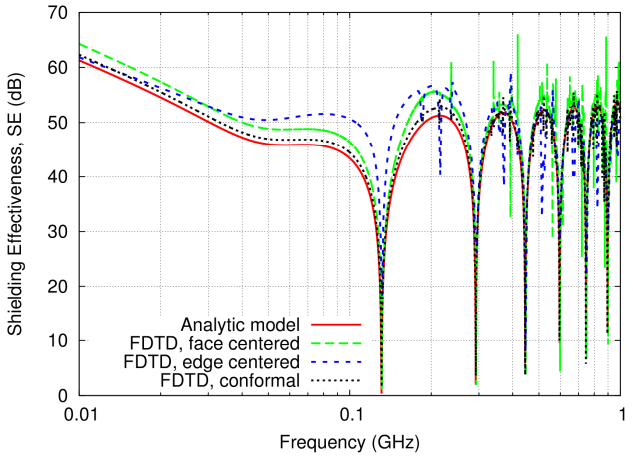

Fig. 4. Shielding effectiveness at the center of the hollow spherical shell with σ = 1 kS/m and thickness h = 1 mm comparing the analytic solution to the different FDTD methods.

IV. Conclusions

The surface impedance boundary approach is a computationally very efficient and flexible way to incorporate small-scale material properties in a FDTD simulation. It is applicable to a wide range of mesh sizes and to any material for which it is possible to generate a passive and stable rational function impedance matrix model. The face-centered algorithm described here is particularly easy to implement since it automatically deals with most of the complexities associated with corners and interfaces between different surfaces. We have shown that this face centered approach provides more accurate results than the edge-centered method when dealing with stair-cased geometries.

Fundamentally there is still an error due to the stair-cased approximation required when using a structured mesh. The ultimate solution is the use of conformal techniques which provide greater accuracy where the geometrical discretization is a limitation. The computational cost of these may still favor the use of a staircased approximation. For instance, in modelling the shielding analysis of electrically large structures, such as airframes at microwave frequencies.

References

[1] Cole, J. A.; Dawson, J. F. & Porter, S. J. , "Efficient Modelling of Thin Conducting Sheets within the TLM method" , *Computation in Electromagnetics, Third International Conference on (Conf. Publ. No. 420) , no. Conf. Publ. No. 420* , 45-50 , 10--12 April 1996

[2] M. K. Karkkainen and P. M. T. Ikonen, "Finite-difference time-domain modeling of frequency selective surfaces using impedance sheet conditions", IEEE Transactions on Antennas and Propagation, vol. 53, no. 9, pp. 2928-2937, Sept. 2005.

[3] V. Nayyeri, M. Soleimani and O. M. Ramahi, "A method to model thin conductive layers in the finite-difference time-domain method", IEEE Transactions on Electromagnetic Compatibility, vol. 56, no. 2, pp. 385-392, April 2014

[4] S. Dey and R.Mittra, "A locally conformal finite-difference time-domain (FDTD) algorithm for modelling three-dimensional perfectly conducting objects", IEEE Microwave and Guided Wave Letters, vol. 7, pp. 273-275, 1997.

[5] Cabello, M. R.; Angulo, L. D.; Alvarez, J.; Bretones, A. R.; Gutierrez, G. G. & Garcia, S. G. , "A New Efficient and Stable 3D Conformal FDTD" , *IEEE Microwave and Wireless Components Letters , vol. 26, no. 8* , 553-555 , Aug 2016.

[6] M. S. Sarto, "A new model for the FDTD analysis of the shielding performances of thin composite structures", IEEE Transaction on Electromagnetic Compatibility, vol. 41, no. 4, pp. 298–306, 1999.

[7] G. Kobidze, "Implementation of collocated surface impedance boundary conditions in FDTD", IEEE Transactions on Antennas and Propagation, vol. 58, no. 7, pp. 2394 –2403, 2010.

[8] G. Kobidze, "Implementation of collocated surface impedance boundary conditions in FDTD", IEEE Transactions on Antennas and Propagation, vol. 58, no. 7, pp. 2394 –2403, 2010.

[9] J. B. Schneider, "Understanding the finite-difference time-domain method", April 5, 2016. Online: http://www.eecs.wsu.edu/~schneidj/ufdtd.

[10] M. S. Sarto, S. Greco and A. Tamburrano, "Shielding effectiveness of protective metallic wire meshes: EM modeling and validation", IEEE Transactions on Electromagnetic Compatibility, vol. 56, no. 3, pp. 615-621, June 2014.

[11] University of Granada UGRFDTD code. Online: http://maxwell.ugr.es/ugrfdtd.

[12] M. R. Cabello, L. D. Angulo, J. Alvarez, I. D. Flintoft, S. A. Bourke, J. F. Dawson, R. G. Martin and S. G. Garcia, "A hybrid Crank-Nicolson FDTD subgridding boundary condition for lossy thin-layer modeling", *IEEE Transactions on Microwave Theory and Techniques*, under review.

[13] M. R. Cabello, L. D. Angulo, J. Alvarez, A. R. Bretones, G. G. Gutierrez and S. G. Garcia, "A new efficient and stable 3D conformal FDTD", *IEEE Microwave and Wireless Components Letters*, accepted for publication.